COMPUTATION OF HEAT TRANSFER OF A PLANE TURBULENT JET IMPINGING A MOVING PLATE

by

Dahbia BENMOUHOUB* * and Amina MATAOUI

Theoretical and Applied Laboratory of Fluid Mechanics, University of Science and Technology Houari Boumedienne, Algiers, Algeria

Original scientific paper
DOI: 10.2298/TSCI111027101B

This study examines the performance of one point closure turbulence models in predicting of heat and momentum transfer of impinging flows. The scope of this paper is limited to impinging jet on a moving wall and heat transfer. The impinging distance is fixed to 8 thickness of the nozzle (8e) for this study. Two parameters are considered: the jet exit Reynolds number ($10000 \le Re \le 25000$) and the jet-surface velocity ratio ($0 \le R_{sj} \le 4$). The flow field structure at a given surface-to-jet velocity ratio is independent of the jet Reynolds number, a slight modification of the flow field is observed for low surface-to-jet velocity ratio ($R_{sj} < 0.25$) whereas at higher ratios $R_{sj} > 0.25$, the flow field is significantly modified. Good agreement with experimental results is obtained for surface-to-jet velocity ratio $0 \le R_{sj} \le 2$. The purpose of this paper is to consider the case of higher of surface-to-jet velocity $R_{sj} > 2$. A further study of heat transfer shows that at the stagnation points the local heat transfer coefficient have a maximum value. The local Nusselt number at the impinging region tends to decrease significantly when $R_{sj} \le 1.5$. The evolution of average Nusselt number is correlated according to the surface-to-jet velocity ratios for each Reynolds number.

Key words: *impingement jet, moving wall, numerical simulation, turbulence modelling, Nusselt number*

Introduction

The interest to the researchers of prediction of heat and momentum transfer of impinging flows is considerable. Heat transfer of impinging jets has received considerable attention in many benchmarks. Such configurations are used in many industrial and engineering applications (*e. g*. manufacturing, material processing and electronic cooling, drying paper, textiles, and tempering of glass). The possibility of improving the heat transfer is carried out according to the parameters of the interaction. Many workshave detailed this configuration, as: Abramovich [1], Rajaratnam [2], Gutmark and Wygnanski [3], Ramaprian and Chandrasekhara [4], Peng *et al*. [5], and Issa *et al*. [6].

The flow of turbulent jet impingement on a still surface generates three regions: the free jet region, the impingement region, and the wall jet region. The addition of surface motion adds one more level of complexity to the problem. Few studies have reported the effect of the

* Corresponding author; e-mail:benmouhoub_d@yahoo.com

impingement surface motion on the flow field and heat transfer. Subba Raju and Schlunder [7] performed an experimental study on an impinging jet a moving belt. The mean heat transfer coefficient was calculated on the basis of the length of impingement surface for different nozzle-to-surface spacing, several Reynolds numbers and various surface velocity V_s between 0.15 m/s and 5.5 m/s. They found that the mean Nusselt number increases with the surface velocity, and is 1.5-2.0 times larger then that of the stationary wall and then remains constant. Van Heiningen *et al*. [8] have considered a turbulent plane jet impinging a rotating drum at low tangential velocity less than 2% of the jet exit velocity. They compared their results with those found by Gardon and Akfirat [9] for a still plate and deduced that wall convective heat transfer are not influenced by the low jet-drum velocity ratios. The flow field of confined turbulent slot air jet impinging normally on a flat surface was investigated experimentally by Senter and Solliec [10]. The experiments were conducted for a nozzle-to-plate spacing of 8 slot nozzle widths, at three Reynolds number (5300, 8000, and 10600) and four surface-to-jet velocity ratios (0, 0.25, 0.5, and 1.0). The measurements of the mean velocities and turbulent quantities are presented in the following main characteristic regions of the jet. It appears that the flow field patterns at a given surface-to-jet velocity ratio are independent of the jet Reynolds number between 5300-10600. A minor modification of the flow field is observed for the surface-to-jet velocity ratio of 0.25 whereas at higher ratios of 0.5 and 1, the flow field is significantly affected.

Numerical modelling of turbulent planar air jet on a rectangular duct was performed by Huang *et al*. [11]. They have found that, when the plate velocity is higher, Nusselt numbers becomes smaller in the vicinity of the wall, when the wall velocity is opposed to the flow and is higher where the surface motion and the flow are in the same direction. Zumbrunnen [12] and Chen *et al*. [13] have shown that the movement of the impingement surface influences significantly the flow structure and heat transfer characteristics. However, they had considered a numerical model for convective heat transfer within an array submerged planar laminar jets impinging a moving hot surface with uniform heat flux. Zumrunnen *et al*. [14] have developed an analytical study for a plane laminar jet impinging a moving surface. They show that the increasing of the plate velocity produce somewhat uniform heat transfer distribution away from the stagnation point. Chattopadhayay *et al.* [15] investigated numerically turbulent heat transfer of an array of slot jets impinging a moving plate by large eddy simulation (LES), for jet exit Reynolds number ranging between 500 and 3000 and for several surface-jet velocities ratios R_{sj} (0, 0.5, 1, and 2). They concluded that the Nusselt number distribution over the plate becomes more uniform when the total heat transfer and plate velocity diminish. Similar conclusions were reported by Chattopadhayay and Saha [16]for laminar heat transfer of an array of impinging slot jets on a moving plate for a jet exit Reynolds number between 100-200. Later, Chattopadhayay and Saha [17] by LES investigates the turbulent flow and heat transfer by a single slot jet impingement a moving hot plate. They focus their study on the flow structure, velocity profiles, and turbulent stresses distribution. The heat transfer induced by impinging jet on a moving wall was investigated numerically by Senter [18] using the standard k-ε turbulence model. The nozzle-to-plate spacing (H) is eight slot nozzle thickness (e) for jet exit Reynolds number Re = = 10600 and for jet to plate velocities ratios of 0, 0.25, 0.5, and 1.0. A good agreement was obtained with Gardon and Akfirat [9] for immobile plate case. This study showed that the local Nusselt number in impact area tends to decrease significantly with the increasing of the plate velocity. Sharif and Benerjee [19] by using CFD Fluent code investigated a numerical study based on the standard k-ε turbulence model combined to the enhanced wall treatment. Three parame-

ters were considered: the jet exit Reynolds number ($5000 \le \mathrm{Re} \le 20000$) , impinging distance ($6e \le H \le 8e$) and the jet-surface velocity ratio ($0 \le R_{sj} \le 2$).They show that the local Nusselt number along the moving plate reaches a maximum value nearby the stagnation point for low velocities ratios which can be explained by the thinning of dynamical and thermal boundary layers. At a given plate velocity, the average Nusselt number along the plate increases when the jet exit Reynolds number increases.

The studies [20, 21] focus on laminar multiples jets impinging a moving wall.

Therefore in this work, all phenomena about the plane turbulent jet impinging normally on a moving flat wall were detailed for jet-plate velocity ratio $0 \le R_{sj} \le 4$.

Methodology

Turbulence model

Mass conservative equation (eq. 1), steady Reynolds average Navier stokes (SRANS) equations (eq. 2) coupled to the averaged energy equation (eq. 3) of the turbulent incompressible flows are:

– mass conservation equation

$$\frac{\partial U_i}{\partial x_i} = 0 \tag{1}$$

– momentum conservation equation

$$\rho U_j \frac{\partial U_i}{\partial x_j} = \frac{\partial P}{\partial x_i} + \frac{\partial}{\partial x_j}\left(\mu \frac{\partial U_i}{\partial x_i} - \rho \overline{u_i u_j} \right) \tag{2}$$

– energy conservation equation

$$\rho U_i \frac{\partial T}{\partial x_i} = \frac{\partial}{\partial x_i}\left(\frac{\mu}{\mathrm{Pr}} \frac{\partial T}{\partial x_i} - \rho \overline{u_i \theta} \right) \tag{3}$$

where P, T, and U_i are the mean pressure, temperature and velocity components, respectively, θ and u_i are the fluctuating temperature and velocity components, respectively. x_i is the co-ordinate direction and ρ and μ are the fluid density and dynamic viscosity, respectively.

The Reynolds stress component and correlations between the velocity and temperature fluctuations require a closure.The one point closure turbulent models are based on the concept of Prandtl-Kolmogorov's turbulent viscosity. Thus, the Reynolds stress tensor and the correlation of the velocity and temperature fluctuations are deduce from Boussinesq assumption:

$$\overline{u_i u_j} = \frac{2}{3} k \delta_{ij} - \nu_t (U_{i,j} + U_{j,i}) \tag{4}$$

$$-\rho \overline{u_i \theta} = \alpha_t \frac{\partial T}{\partial x_i} \tag{5}$$

By analogy with molecular transport, the turbulent Prandtl number for thermal transport equation can be deduced through eq. (6):

$$\sigma_T = \frac{\mu_t}{\alpha_t} \tag{6}$$

The closure energy-specific dissipation (k-ω) one point closure turbulence model is used in this paper.

The first formulation of k-ω model was developed by Wilcox [22]. It solves two transport equations, for the first one the turbulent kinetic energy k (eq. 7), and second one is the turbulent frequency ω, (eq. 8):

$$\rho U_j \frac{\partial k}{\partial x_j} = \frac{\partial}{\partial x_j}\left[\left(\mu + \frac{\mu_t}{\sigma_k}\right)\frac{\partial k}{\partial x_j}\right] + \mu_t\left[\frac{\partial U_i}{\partial x_j} + \frac{\partial U_j}{\partial x_i}\right]\frac{\partial U_i}{\partial x_j} - \rho\omega k \tag{7}$$

$$\rho U_j \frac{\partial \omega}{\partial x_j} = \frac{\partial}{\partial x_j}\left[\left(\mu + \frac{\mu_t}{\sigma_\omega}\right)\frac{\partial \omega}{\partial x_j}\right] + C_{\omega 1}\mu_t\left[\frac{\partial U_i}{\partial x_j} + \frac{\partial U_j}{\partial x_i}\right]\frac{\partial U_i}{\partial x_j}\omega - C_{\omega 2}\rho\omega^2 \tag{8}$$

The turbulent viscosity ν_t is deduced by:

$$\nu_t = \frac{k}{\omega}$$

The empirical constants of the above equations are: $C_\mu = 0.09$, $C_{\omega 1} = 0.555$, $C_{\omega 2} = 0.833$, $\sigma_k = 2.0$, $\sigma_\omega = 2.0$ and $\sigma_T = 1.0$.

Numerical method

The steady conservation equations for incompressible 2-D in Cartesian co-ordinate are solved with the finite volume method [23]. The finite volume method requires the following conservative form:

$$\frac{\partial}{\partial x_j}(\rho U_i \phi) = \frac{\partial}{\partial x_j}\left[\Gamma_\phi \frac{\partial \phi}{\partial x_j}\right] + S_\phi, \quad j = 1, 2 \tag{9}$$

where ϕ is one of the dependent variables U, V, T, k, and ω, Γ_ϕ and S_ϕ are the corresponding turbulent diffusion coefficient and source term, respectively. The terms of Γ_ϕ and S_ϕ are deduced from eq. (9) for each variable ϕ (see tab. 1.)

Table 1. Diffusion coefficients and source terms in the generic transport eq. (9)

Equation	ϕ	Γ_ϕ	S_ϕ
Continuity	1	0	0
x-momentum	U	$\mu_{\text{eff}} = \mu_t + \mu$	$\left[-\frac{\partial p}{\partial x} + \frac{\partial}{\partial x}\left(\mu_{\text{eff}}\frac{\partial U}{\partial x}\right) + \frac{\partial}{\partial y}\left(\mu_{\text{eff}}\frac{\partial V}{\partial x}\right)\right]$
y-momentum	V	$\mu_{\text{eff}} = \mu_t + \mu$	$\left[-\frac{\partial p}{\partial x} + \frac{\partial}{\partial x}\left(\mu_{\text{eff}}\frac{\partial U}{\partial y}\right) + \frac{\partial}{\partial y}\left(\mu_{\text{eff}}\frac{\partial V}{\partial y}\right)\right]$
Energy	T	$\frac{\mu}{\text{Pr}} + \frac{\mu_t}{\sigma_T}$	0
Kinetic energy	k	$\mu + \frac{\mu_t}{\sigma_k}$	$\mu_t\left\{\left(\frac{\partial U}{\partial y} + \frac{\partial V}{\partial x}\right)^2 + 2\left[\left(\frac{\partial U}{\partial x}\right)^2 + \left(\frac{\partial V}{\partial y}\right)^2\right]\right\} - \rho\omega k$
Specific dissipation rate	ω	$\mu + \frac{\mu_t}{\sigma_\omega}$	$C_{\omega 1}\mu_t\left\{\left(\frac{\partial U}{\partial y} + \frac{\partial V}{\partial x}\right)^2 + 2\left[\left(\frac{\partial U}{\partial x}\right)^2 + \left(\frac{\partial V}{\partial y}\right)^2\right]\right\}\omega - C_{\omega 2}\rho\omega^2$

The convection and diffusion terms are discretized using the POWER LAW schemes. The pressure-velocity coupling is realized by SIMPLEC algorithm. The solution is considered converged when the normalized residual of each variable is less than 10^{-6}.

The geometry and boundary conditions are summarized in fig. 1. The jet exit velocity U_j is varied giving a Reynolds number, based on the nozzle width e (where ν is the kinematic viscosity) ranging from 10000 to 25000. The moving wall is displaced at the velocity U_0 corresponding to the surface-to-jet velocity ratio R_{sj} defined by: $R_{sj} = U_0/V_j$.The impinging distance H is fixed to 8e in this study. The jet at the exit and the upper plate are maintained at ambient temperature T_C but the moving one is heated at T_H (T_C = 293 K and T_H = 313 K).

A 2-D structural non-uniform grid has been generated. A sufficiently fine grid is managed near the jet and the wall, where prevails a very high gradient of each variable (fig. 2).

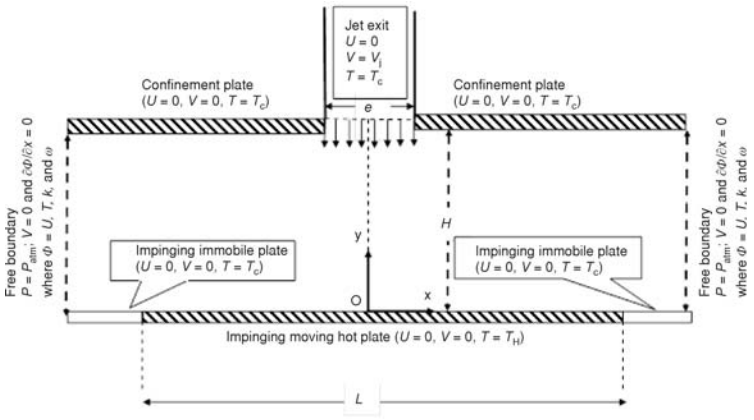

Figure 1. Configuration and boundary conditions

Impinging jet flows are mainly influenced by the near-wall turbulence behaviour. The local turbulence Reynolds number y^+ is used to show the near wall behavior. Qualitatively, fig. 3 shows similar profiles to those of Beaubert and Viazzo [24]. At several section, the tangential velocity U^+ profiles are characterized by three zones:

– viscous sublayer ($y^+ < 5$),
– buffer layer or blending region ($5 < y^+ < 26$), and
– fully turbulent or log-law region ($y^+ > 26$).

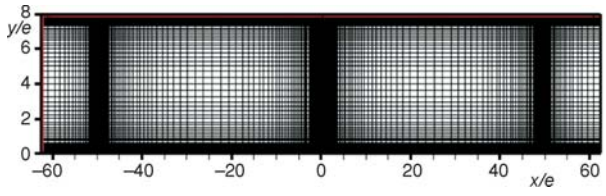

Figure 2. Grid arrangement

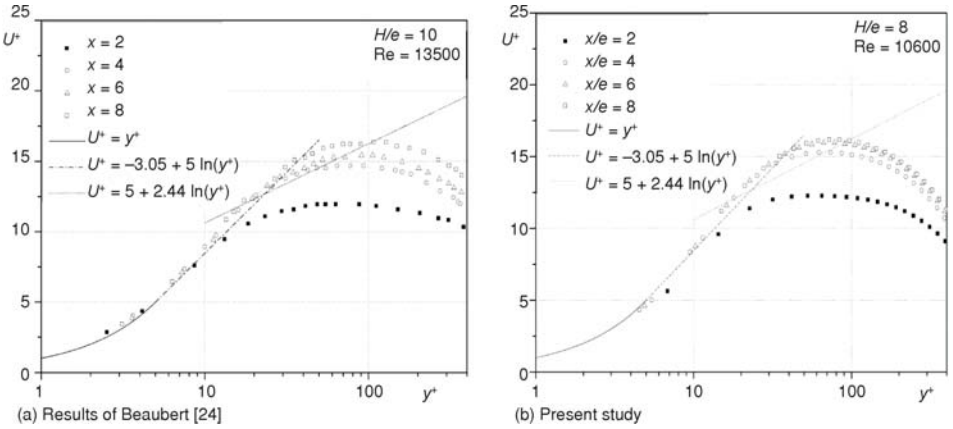

Figure 3. Near wall treatment for *y/e* = 2, 4, 6, and 8

In the vicinity of the wall, viscous damping reduces the tangential velocity fluctuations, while kinematic blocking reduces the normal fluctuations. Towards the outer part of the near-wall region, the turbulence grows rapidly by the production of turbulent kinetic energy due to the large gradients in mean velocity.

Results and discussion

Validation of numerical models

The mean velocities components (U/V_j) and (V/V_j), are in good agreement with experimental data obtained by PIV [18]. The profile of fig. 4 for the case (a), relative to the still wall case are symmetric. For $R_{sj} = 0.5$, the effect of the moving wall is visible by the asymmetry of velocity profiles.

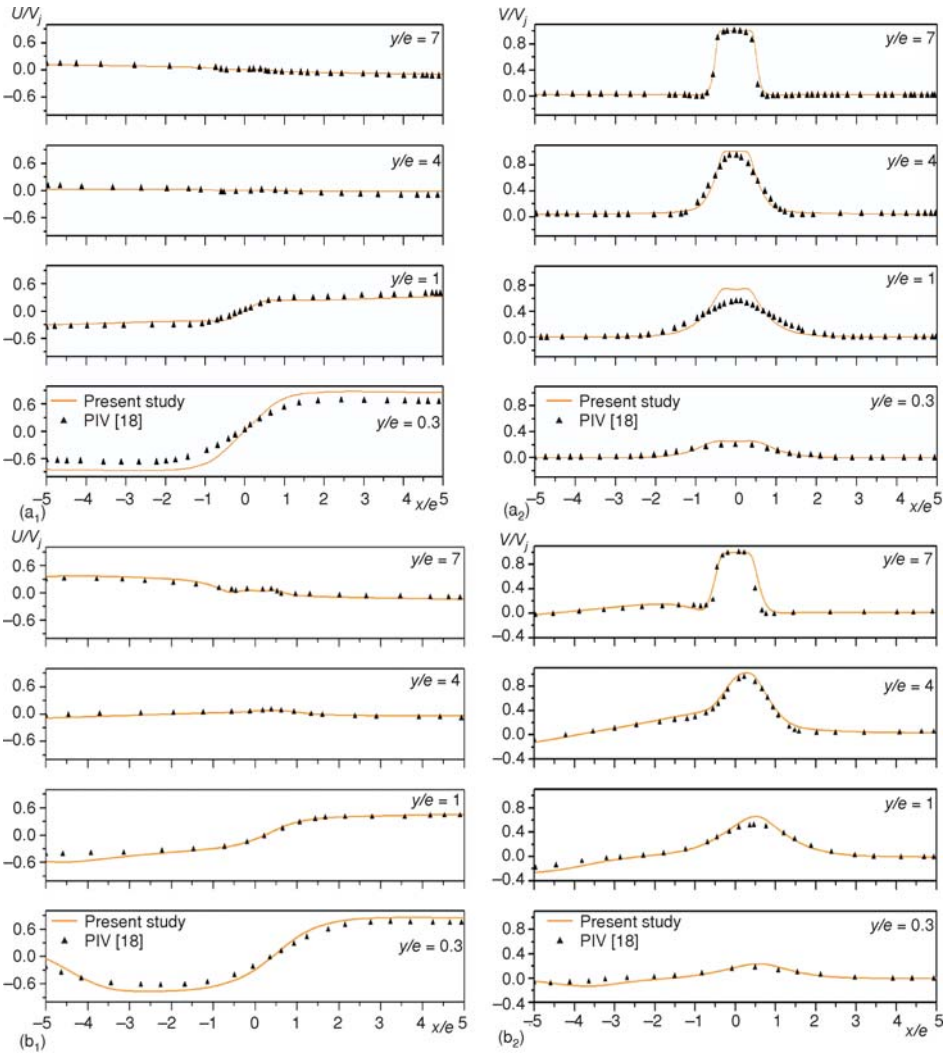

Figure 4. Mean velocities components U/V_j and V/V_j (H/e = 8, Re = 7850; (a) R_{sj} = 0, (b) R_{sj} = 0.5

The computed streamlines contours are plotted in fig. 5, corresponding to surface-to-jet velocities ratios (R_{sj} = 0 and 0.5) for Re = 10600. The results are compared to experimental measurements (PIV) and numerical prediction by k-ε model of Senter [18]. Good agreement is obtained. The location of the stagnation point was found with a good precision by calculation. For R_{sj} = 0, corresponding to the stationary plate. Besides, the center of the re-circulation obtained by calculation is slightly shifted to that of the experiment. The first case in fig. 5 presents a typical turbulent slot jet confined and impinging on a stationary surface. Two identical eddies are observed. The second case (R_{sj} = 0.5), a third contra-rotating eddy appears at the left part of the moving wall. This new re-circulation compresses the size of the left principal vortex which deflects the jet towards the right part of the mobile wall.

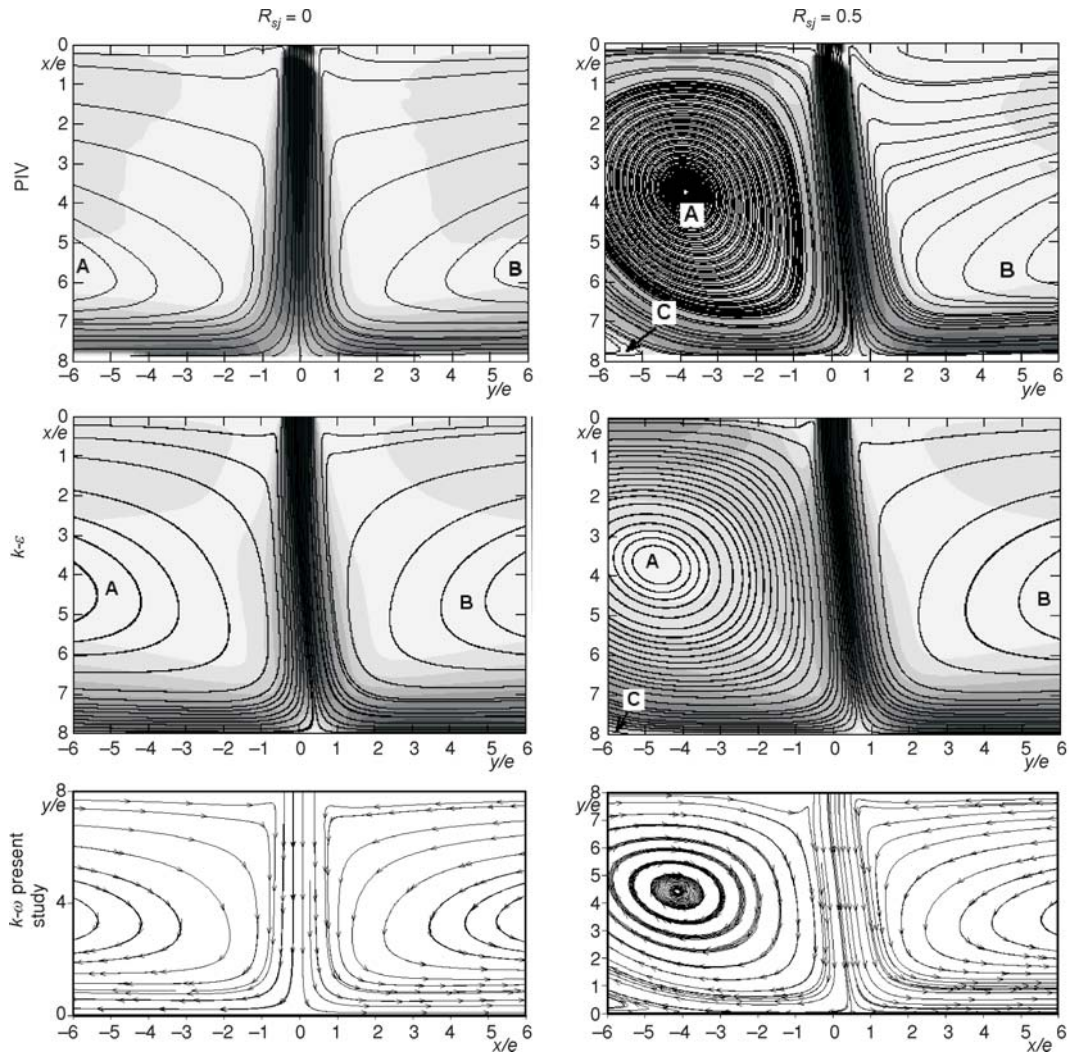

Figure 5. Streamlines contours comparison *H/e* = 8, Re = 10600

The variation of the local Nusselt number along the impingement plate Nu(x) is calculated from the temperature gradient along the hot plate by:

$$\mathrm{Nu}(x) = -\left(\frac{e}{T_\mathrm{H} - T_\mathrm{C}}\right)\left(\frac{\partial T}{\partial y}\right)_{\mathrm{y\text{-}wall}} \tag{10}$$

and the average Nusselt number along the moving wall is also deduced from eq. 11:

$$\overline{\mathrm{Nu}} = \frac{1}{L}\int_{-1/2}^{1/2} \mathrm{Nu}(x)\mathrm{d}x \tag{11}$$

Figure 6(a) represents the computed local Nusselt number for the case of the stationary impingement plate ($R_{sj} = 0$) compared to the experimental results of Gardon and Akfirat [9] and to the numerical results of Senter [18] based on the k-ε model for $H/e = 8$ at Re = 11000. According to these data, we can say that the prediction of Nusselt number by the standard k-ω model is more accurate than the k-ε model.

Figure 6 (b, c, and d) shows the comparison of the computation based on standard k-ω model to those of Senter [18] of the local Nusselt number evolution along the moving wall for two the surface-to-jet velocity ratios , $R_{sj} = 0.25$, 0.5, and 1 at Re = 10600. A good agreement between the two predictions is obtained.

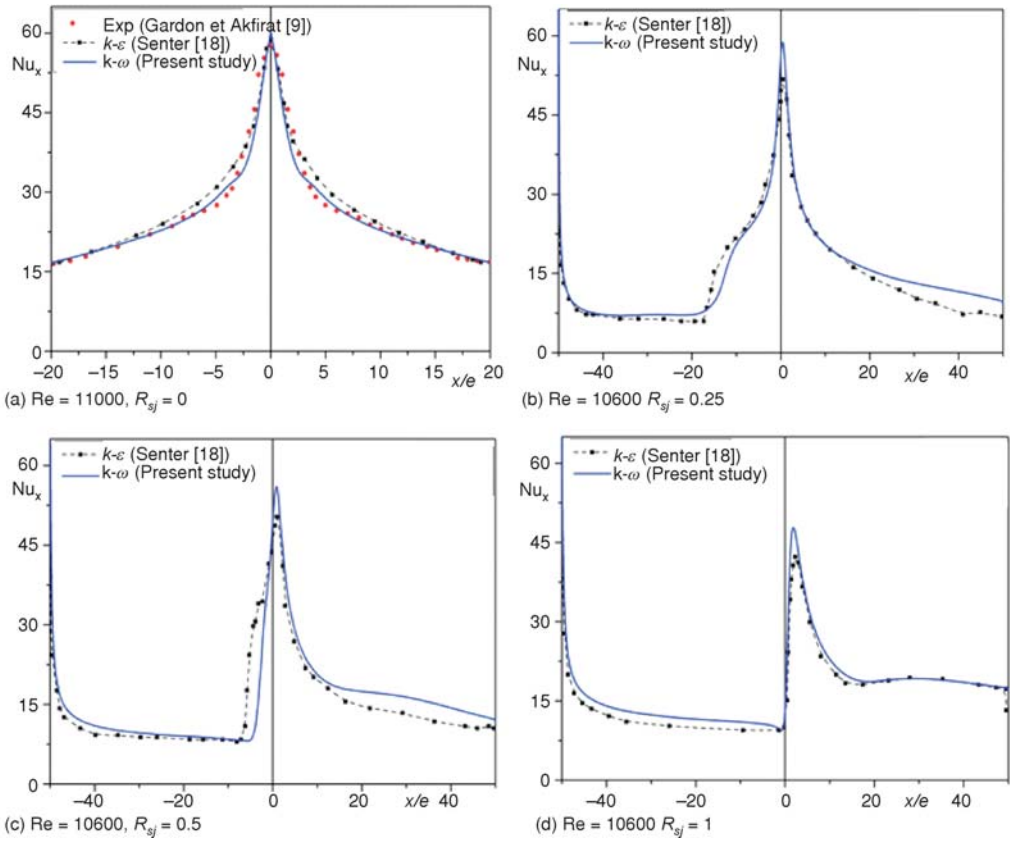

Figure 6. Local Nusselt number distribution along the hot wall with H/e = 8

Effect of the surface-to-jet velocity on the local Nusselt number evolution

Figure 7 shows the local Nusselt number evolution along the moving wall, for various values of surface-to-jet velocity ratios R_{sj} ($0 \le R_{sj} \le 4$) at Re = 10600. Figure 7(b) is an enlargement of the fig. 7(a). From these figures we can give the following explanations:

– For $R_{sj} = 0$: the curve has the shape of a symmetrical bell, it characterizes the distribution of the local number of Nusselt of the flow of the plane jet impinging perpendicularly an immobile plate. The maximum value matches exactly with the stagnation point of the jet, on both sides by the jet axis, then it decreases progressively and symmetrically.
– For $0.25 \le R_{sj} \le 1.5$ one notes that:
  - When the velocity ratio R_{sj} increases, the maximum value of the local Nusselt number decreases and the stagnation point (x_0/e) is shifted in the same direction of the movement of the mobile plate.
  - A reduction of the local Nusselt number is observed in the left part of the plate for each velocity ratio R_{sj}, this decrease is related to the creation of the new recirculation (separation of the fluid of the wall) [18, 19].

  The Nusselt number distribution at the left edge of the moving plate (x/e = –50) is characterized by a pronounced peak which increases when R_{sj} augments. This maximum can be explained by the discontinuity of the configuration located between mobile surface and the immobile left wall [18].This phenomenon does not appear at the right edge (x/e = 50) because the jet flow is driven in the same direction of the plate motion, contrarily to the left edge (x/e = –50) where the flow is opposed the plate movement.
  - The Nusselt number increases on the right part of the plate when R_{sj} increases by the effect of the gradual jet deflection.
– For $1.75 \le R_{sj} \le 4$; the curves of the local Nusselt number distribution are practically linear (absence of obvious peak) because the flow leaves entirely the plate.

The locations and the maximum Nusselt number values for the various surface-to-jet velocity ratios R_{sj} are referred in tab. 2.

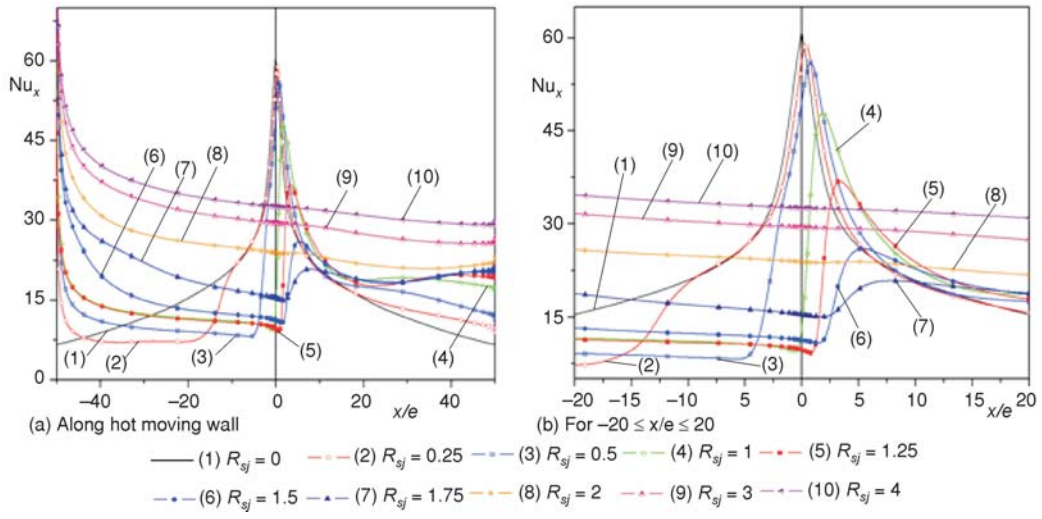

Figure 7. Distribution of local Nusselt number with H/e = 8 at Re = 10600, $0 \le R_{sj} \le 4$

Table 2. Effect of surface-to-jet velocity on the maximum values of the local Nusselt number and the position of stagnation point Re = 10600, *H/e* = 8

R_{sj}	0	0.25	0.5	1	1.25	1.5
x_0/e	0	0.434	0.784	1.837	3.450	5.552
Nu_{max}	61.047	58.796	56.000	47.849	36.796	25.945

Effect of the Reynolds number on the evolution of the local Nusselt number

The effect of the Reynolds number on the distribution of the local Nusselt number is represented in fig. 8, for jet exit Reynolds number, ranging from 10000 to 25000 and for two cases of surface-to-jet velocity ratios (R_{sj} = 0.5 and 1).

Regardless of the Reynolds numbers range considered in this study, for a given surface velocity R_{sj}, the evolutions of the local Nusselt number are similar. Their maximum values increase with the Reynolds number but its location does not seem to be influenced by the Reynolds number.

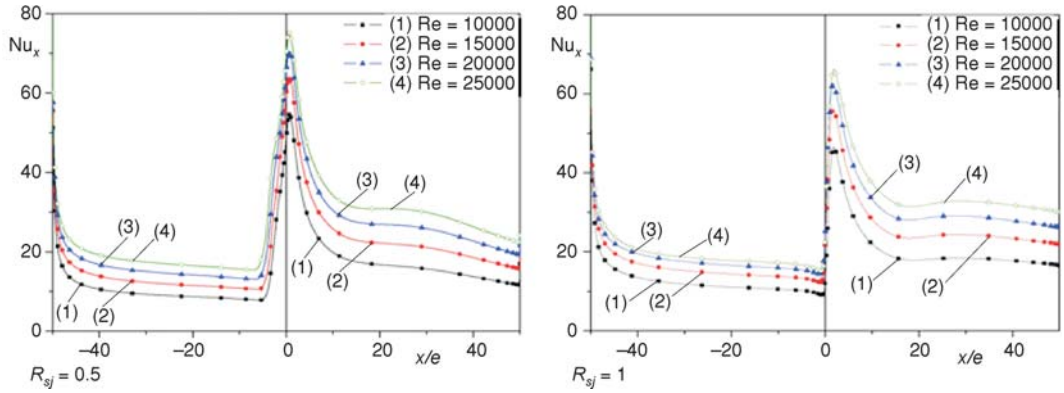

Figure 8. Effect of Reynolds number on the evolution of local Nusselt number

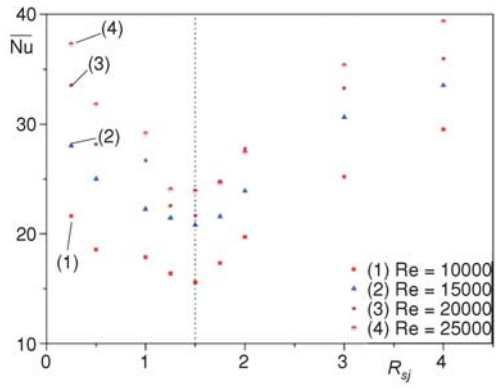

Figure 9. Variation of the average Nusselt number

Evolution of average Nusselt number

Figure 9 illustrates the average Nusselt number evolution according to the surface-to-jet velocity ratios at several Reynolds numbers, between –20*e* and 20*e* in order to take into account only the effect of the impinging region. The average Nusselt number decreases when the surface-to-jet velocity ratios is up to 1.5 ($R_{sj} \leq 1.5$), then it increases with the increase the surface-to-jet velocity ratios.

The average Nusselt number evolution according to the surface-to-jet velocity ratios for each Reynolds number is correlated by power expression (tab. 3):

$$\overline{\mathrm{Nu}} = \gamma R_{sj}^{\delta}$$

For $0.25 \le R_{sj} \le 1.5$: δ is equal to –0.166, but γ varies between 17.368 and 27.437 depending on the Reynolds number.

For $1.75 \le R_{sj} \le 4$: δ is equal to 0.646 but γ varies between 12.227 and 17.944 depending on the Reynolds number.

Table 3. Correlation of the average Nusselt number according R_{sj}

Re \ R_{sj}	$0.25 \le R_{sj} \le 1.5$	$1.75 \le R_{sj} \le 4$
10000	$\overline{\mathrm{Nu}} = 17.368 R_{sj}^{-0.166}$	$\overline{\mathrm{Nu}} = 12.227 R_{sj}^{0.646}$
15000	$\overline{\mathrm{Nu}} = 22.263 R_{sj}^{-0.166}$	$\overline{\mathrm{Nu}} = 14.764 R_{sj}^{0.646}$
20000	$\overline{\mathrm{Nu}} = 25.475 R_{sj}^{-0.166}$	$\overline{\mathrm{Nu}} = 16.579 R_{sj}^{0.646}$
25000	$\overline{\mathrm{Nu}} = 27.437 R_{sj}^{-0.166}$	$\overline{\mathrm{Nu}} = 17.944 R_{sj}^{0.646}$

The relative error is deduced thought the difference between the calculate Nu value and the computed Nu from the correlation by:

$$\frac{\overline{\mathrm{Nu}}_{\mathrm{cal}} - \overline{\mathrm{Nu}}_{\mathrm{corr}}}{\overline{\mathrm{Nu}}_{\mathrm{cal}}}$$

The relative error of the correlations of average Nusselt number according to surface-to-jet velocity ratios R_{sj}, compared calculations (k-ω) are gathered in tab. 4. The error is great for high value of Reynolds number and the big surface-to-jet-velocity ratios.

Table 4. Relative error of the correlations of average Nusselt number according to R_{sj}

	$\frac{\overline{\mathrm{Nu}}_{\mathrm{cal}} - \overline{\mathrm{Nu}}_{\mathrm{corr}}}{\overline{\mathrm{Nu}}_{\mathrm{cal}}}$ [%]								
Re \ R_{sj}	0.25	0.5	1	1.25	1.5	1.75	2	3	4
10000	1.15	5.01	2.73	2.28	4.30	1.30	2.86	1.34	1.46
15000	3.51	4.94	2.99	4.42	8.03	1.80	3.30	2.01	7.76
20000	4.35	1.47	4.54	8.87	10.02	3.96	6.51	1.38	12.89
25000	7.36	3.09	5.90	10.49	6.69	5.58	6.01	4.04	17.67

Conclusions

The k-ω turbulence model has been used to predict the flow resulting from the orthogonal impingement of two-dimensional plane jet on a moving wall. The flow structure simulation turbulence model is compared with experimental results have been obtained using a finite volume numerical method. Results show good qualitative and quantitative agreement with measurements and previous numerical works.

The effect of Reynolds number and surface-to jet velocity ratio on heat transfer has been analyzed. The influence of the moving surface velocity on the global structure and heat transfer of such a flow has been also captured. The calculation of time-averaged velocities and Nusselt number in this case will provide comparisons with numerical works. The heat transfer on the impingement surface is evidenced by the flow with the increasing of the moving surface velocity. Certainly, the deviation of the location of the stagnation point from the jet exit axis will

generate an important variation on the heat transfer. For high velocity ratios, no stagnation point is observed because there is a full detachment of the flow from the wall. Many correlations are proposed for the average Nusselt number evolution according to the surface-to-jet velocity ratios for each Reynolds number.

Nomenclature

e – slot nozzle width, [m]
H – impingement distance, [m]
k – kinetic energy of turbulence, [m^2s^{-2}]
L – length of the impingement plate, [m]
Nu_x – local Nusselt number, [–]
$\overline{Nu}$ – average Nusselt number, [–]
P – mean pressure, [Pa]
Pr – Prandtl number, [–]
Re – Reynolds number, [–]
R_{sj} – surface-to jet velocity ratio, [–]
T – mean temperature, [K]
U – mean velocity in the x-direction, [ms^{-1}]
U^+ – non-dimensional velocity, [–]
U_0 – velocity of the impingement surface, [ms^{-1}]
U_i – mean velocity components, [ms^{-1}]
U_j – nozzle jet velocity exit, [ms^{-1}]
u_j – fluctuating velocity components, [ms^{-1}]
V – mean velocity in the y-direction, [ms^{-1}]
x_i – co-ordinate directions, [m]
y^+ – non-dimensional distance, [–]

Greek symbols

μ – dynamic viscosity of fluid, [$kgm^{-1}s^{-1}$]
μ_t – turbulent eddy viscosity, [$kgm^{-1}s^{-1}$]
ρ – fluid density, [kgm^{-3}]
ω – specific dissipation rate, [s^{-1}]

Subscripts

C – cold temperature
H – hot temperature
t – turbulent

Reference

[1] Abramovich, G. N., *The Theory of Turbulent Jets*, MIT Press, Cambridge, Mass., USA, 1963
[2] Rajaratnam, N., *Turbulent Jets*, Elsevier Scientific Publishing Company, 1976
[3] Gutmark, E., Wygnanski, I., The Planar Turbulent Jet, *J. Fluid Mech, 73* (1976), 3, pp. 465-495
[4] Ramaprian, B. R., Chandrasekhara, M., LDA Measurements in Plane Turbulent Jets, *J. Fluids Eng., 107* (1985), 2, pp. 264-271
[5] Xu, P., *et al*., Heat Transfer under a Pulsed Slot Turbulent Impinging Jet at Large Temperature Differences, *Thermal Science, 14* (2010), 1, pp. 271-281
[6] Issa, R. J., Heat Transfer Performance of Oil Jet Impinging on a Downward Facing Stainless Steel Plate, *Thermal Science, 15* (2011), 2, pp. 397-408
[7] Subba Raju, K., Schlunder, E. U., Heat Transfer between an Impinging Jet and a Continuously Moving Surface, *Warme-und Stoffubertragung, 10* (1977), 10, pp. 131-136
[8] Van Heiningen, A. R. P., *et al*., Flow and Heat Transfer Characteristics of Turbulent Slot Impinging on a Moving Wall, *Proceedings*, 1st Symposium Turbulent Shear Flow, Penn-State University, College Park, Penn., USA, 1977, Vol. 1, pp. 3.9-3.15
[9] Gardon, R., Akfirat, J. C., Heat Transfer Characteristics of Impinging Two-Dimensional Air Jets, *Journal Heat Transfer, Transactions of the ASME, 88* (1966), 1, pp. 101-108
[10] Senter, J., Solliec, C., Flow Field Analysis of a Turbulent Slot Air Jet Impinging on a Moving Flat Surface, *International Journal of Heat and Fluid Flow, 28* (2007), 4, pp. 708-719
[11] Huang, P. G., *et al*., Numerical Prediction of Fluid Flow and Heat Transfer under a Turbulent Impinging Slot Jet with Surface Motion and Crossflow, *Transactions of the ASME, 33* (1984), pp. 1-8
[12] Zumbrunnen, D. A., Convective Heat and Mass-Transfer in the Stagnation Region of a Laminar Planar Jet Impinging on a Moving Surface, *Journal of Heat Transfer, 113* (1991), 3, pp. 563-570.
[13] Chen, J., *et al*., Numerical Analysis of Convective Heat Transfer from a Moving Plate Cooled by an Array of Submerged Planar Jets, *Numerical Heat Transfer, 26* (1994), 2, pp. 141-160
[14] Zumbrunnen, D. A., *et al.*, Laminar Boundary Layer Model of Heat Transfer Due to a Nonuniform Planer Jet Impinging on a Moving Plate, *Warme-und Stoffubertragung, 27* (1992), pp. 311-319
[15] Chattopadhyay, H., *et al*., Heat Transfer from a Moving Surface Due to Impinging Slot Jets, *Journal of Heat Transfer, 124* (2002), 3, pp. 433-440

[16] Chattopadhyay, H., Saha, S. K., Simulation of Laminar Slot Jets Impinging on a Moving Surface, *Journal of Heat Transfer, 124* (2002), 6, pp. 1049-1055
[17] Chattopadhyay, H.,Saha, S. K., Turbulent Heat Transfer from a Slot Jet Impinging on a Moving Plate, *International Journal of Heat and Fluid Flow, 24* (2003), 5, pp. 685-697
[18] Senter. J., Experimental and Numerical Analysis of Flow and Convective Heat Transfer in the Case of Plane Jet Impinging a Moving Plate (in French), Ph. D. thesis, Université de Nantes, France, 2006
[19] Sharif, M. A. R., Banerjee. A., Numerical Analysis of Heat Transfer Due to Confined Slot-Jet Impingement on a Moving Plate, *Applied Thermal Engineering, 29* (2009), 2-3, pp. 532-540
[20] Aldabbag, L. B. Y., Mohamad. A. A., A Three Dimensional Numerical Simulations of Impinging Jet Arrays on a Moving Plate, *International Journal of Heat and Mass Transfer, 52* (2009), 21-22, pp. 4894-4900
[21] Aldabbag, L. B. Y., Mohamad, A. A., Effect of Jet-to-Plate Spacing in Laminar Array Jets Impinging, *Heat Mass Transfer, 43* (2007), 3, pp. 265-273
[22] Wilcox, D. C. Turbulence Modeling for CFD, DCW Industries, Inc., La Canada, Cal., USA, 1998
[23] Patankar, S. V., *Numerical Heat Transfer and Fluid Flow*, Series in Computational Methods in Mechanics and Thermal Sciences, Hemisphere Publ. Corp., New York, USA, 1980
[24] Beaubert, F., Viazzo, S., Large Eddy Simulations of Plane Turbulent Impinging Jets at Moderate Reynolds Numbers, *International Journal of Heat and Fluid Flow, 24* (2003), 4, pp. 512-519

Paper submitted: October 27, 2011
Paper revised: June 15, 2012
Paper accepted: June 15, 2012